

Efficient Model Agnostic Approach for Implicit Neural Representation Based Arbitrary-Scale Image Super-Resolution

Young Jae Oh Jihun Kim Tae Hyun Kim
 Hanyang University, Seoul, South Korea
 {naohjae, jihunkim, taehyunkim}@hanyang.ac.kr

Abstract

Single image super-resolution (SISR) has experienced significant advancements, primarily driven by deep convolutional networks. Traditional networks, however, are limited to upscaling images to a fixed scale, leading to the utilization of implicit neural functions for generating arbitrarily scaled images. Nevertheless, these methodologies have imposed substantial computational demands as they involve querying every target pixel to a single resource-intensive decoder. In this paper, we introduce a novel and efficient framework, the Mixture of Experts Implicit Super-Resolution (MoEISR), which enables super-resolution at arbitrary scales with significantly increased computational efficiency without sacrificing reconstruction quality. MoEISR dynamically allocates the most suitable decoding expert to each pixel using a lightweight mapper module, allowing experts with varying capacities to reconstruct pixels across regions with diverse complexities. Our experiments demonstrate that MoEISR successfully reduces up to 73% in floating point operations (FLOPs) while delivering comparable or superior peak signal-to-noise ratio (PSNR).

1. Introduction

Single image super-resolution (SISR), which aims to reconstruct a high-resolution (HR) image from a low-resolution (LR) image, stands as a foundational task in computer vision given its capacity to serve the input for various other vision applications. While the majority of recent super-resolution (SR) techniques utilize PixelShuffle [35] based on the convolutional layers as the decoding function [6, 8, 22, 23, 46, 47], this approach exhibits a notable limitation in that it can only upscale images with a predetermined scale. To address this constraint, arbitrary-scale SR methods [5, 7, 9, 15, 21, 38, 40, 42] have been introduced, most of them incorporating a multi-layer perceptron (MLP) as the decoder.

These methods can handle SR at various target scales,

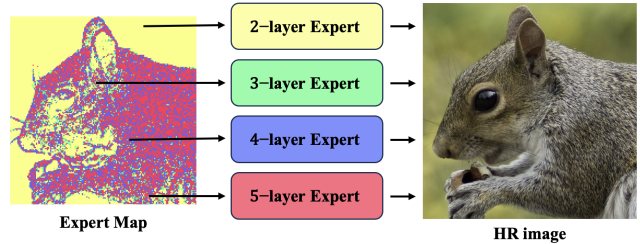


Figure 1. **Expert map from the mapper.** Yellow, green, blue and red pixels in the expert map denote varying levels of reconstruction complexity and their respective associated experts.

which is advantageous since only a single model is required for upscaling images to various resolutions. Nonetheless, these methods place a substantial computational burden, as each pixel necessitates processing by a single resource-intensive MLP decoder. Consequently, they still struggle to provide the essential efficiency required for practical applications, particularly when dealing with the reconstruction of images on a large scale.

In this paper, we introduce the Mixture of Experts Implicit Super-Resolution (MoEISR) for arbitrary-scale SR, achieving a substantial reduction of up to 73% in FLOPs in comparison to prevailing arbitrary-scale SR networks, while delivering comparable or even superior PSNR. To produce high-quality HR images with an emphasis on computational efficiency, our approach involves the joint training of several components. This includes an encoder responsible for generating implicit neural representation (INR), a set of capacity-varying MLP decoders (experts) designed to predict the RGB value of each pixel, and a mapper that assigns pixels to the appropriate expert. The efficacy of MoEISR lies in the mapper, which adeptly assigns experts with varying capacities to each output pixel. Our research is inspired by ClassSR [20] and APE [41], which have demonstrated that leveraging several networks with distinct complexities can enhance SR performance while concurrently reducing the computational burden. In our endeavor to harness the potential of capacity-varying experts while maintaining high reconstruction quality, we integrate the mix-

ture of experts (MoE) scheme [13, 27, 31] which allows the router (mapper) to assign capacity-varying experts to each output pixel. Additionally, we adapt and enhance the loss function initially introduced in ClassSR [20] for the mapper during the training phase.

To illustrate the process, an LR image is passed through the encoder to obtain the INR. This representation is then processed by the mapper, generating an expert map assigning suitable experts to individual output pixels. The obtained INR, along with its corresponding target coordinates, is directed to the assigned expert, predicting the final RGB value. Furthermore, the expert map generated by the mapper offers a distinct visualization of the spatial relationships and relative complexity among pixels. Fig. 1 shows the expert map derived from the provided input image, clearly highlighting the allocation of more computationally heavy experts (e.g. 4-layer and 5-layer experts) along object boundaries characterized by abrupt RGB value transitions, as well as in regions with complex textures. Additionally, given its model-agnostic nature, our MoEISR seamlessly integrates into various INR-based arbitrary-scale SR networks. This integration enhances HR reconstruction quality while reducing computational complexity, demonstrating MoEISR’s adaptability across diverse arbitrary-scale SR frameworks and contributing to the advancement of image upscaling techniques.

We summarize our major contributions as follows:

- We present a model-agnostic approach for INR-based arbitrary-scale SR networks.
- We demonstrate that MoEISR achieves comparable or superior results to existing arbitrary-scale SR networks by utilizing experts with varying capacities in a pixel-wise manner, leading to a reduction of up to 73% in FLOPs.

2. Related Work

Implicit Neural Representation. Significant advancements have been made in computer vision through the utilization of INR. In these approaches, objects are characterized by INRs generated by an encoder. Then, a decoder, MLP in most cases, reconstructs the original object using the representation when queried with coordinates. These methodologies have been employed across diverse tasks in computer vision, including as 3D modeling [3, 10, 18, 26, 28–30, 36], image generation [2, 37], SR [5, 7, 9, 21], and space-time video super-resolution [11]. Nevertheless, many works suffer from high computational complexity due to the enormous number of queries to the decoder. While studies [14, 30] have aimed to reduce computational cost, most of them focus on NeRF [26] and are hard to be applied to other tasks. Our study is dedicated to reducing the computational complexity of INR-based arbitrary-scale SR while preserving its efficacy through the appropriate allocation of capacity-varying decoders to each

individual pixel. Although our approach may appear akin to KiloNeRF [30], it is imperative to discern a crucial distinction. KiloNeRF [30] necessitates thousands of distinct MLPs to various segments of the scene, whereas our method effectively employs at most 4 depth-varying MLPs, reconstructing individual pixels regarding their specific reconstruction difficulties.

Arbitrary-Scale Super-Resolution. Many SR researches [6, 8, 12, 22, 23, 46, 47] were conducted to obtain rich representation power using sophisticated architectural designs and showed great results. Nevertheless, these methodologies have encountered a significant challenge in that they are inherently restricted to upscaling to a fixed scale, necessitating the creation of multiple scale-specific trained models to generate HR images at various scales. To overcome the issue, SR approaches with arbitrary up-scale factor [5, 7, 9, 15, 21, 38, 40, 42] have been introduced. Similar to how SRCNN [12] pioneered the integration of deep learning within the field of SR, MetaSR [15] proposed a groundbreaking development by introducing the first innovative approach to upscaling images at arbitrary scales using a single trained model. Following the footsteps, studies such as ArbSR [40] and SRWarp [38] have been introduced. LIIF [9] tried to harness implicit neural functions to upscale images to arbitrary scales. While this method demonstrated promising results, it encountered challenges in accurately preserving fine details when subjected to a large upscale factor. Subsequently, LTE [21] was introduced with the aim of capturing intricate texture details within an image. This improvement was achieved by learning the dominant frequencies of images. However, it also required a huge amount of computation since every output pixel needed to be queried using a single resource-intensive MLP decoder. More recent researches such as CLIT [7] and CiaoSR [5] further improved the reconstruction ability of arbitrary-scale SR but still suffers the aforementioned problem. In contrast, our research introduces a novel approach that initially generates a map to specify which pixel should be processed by which one of the capacity-varying decoders. This meticulous assignment ensures that the INR is channeled through its most suitable decoder, thus allowing for highly accurate pixel value predictions while significantly reducing computational demands.

Semantic-Aware Image Restoration. In order to achieve better image restoration results, reconstructing the texture details of an image is indispensable. Many studies [32, 43, 44, 48] partitioned image regions and processed them with varying parameters, signifying a growing trend in image processing and restoration to tailor treatment to specific regions or components within an image. More recently, ClassSR [20] proposed difficulty-aware SR by using conventional SR networks with varying capacity to reduce the FLOPs required to reconstruct an image by attaching

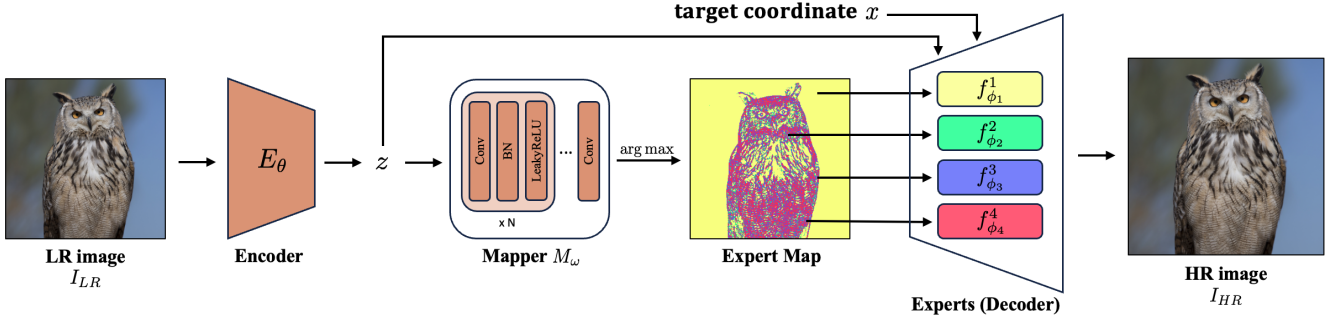


Figure 2. **Arbitrary-scale SR with MoEISR.** Implicit neural representation (z) from the encoder (E_θ) goes through the mapper (M_ω), creating an expert map assigning the most suitable expert to each output pixel. Finally, z along with target coordinate x is passed to the designated decoder ($f_{\phi_j}^j$) predicting the RGB value of the queried pixel.

a class module. Although ClassSR [20] demonstrated significant potential, it necessitated a three-step training procedure and relied on a pre-trained SR network’s ability to accurately classify image regions based on their level of reconstruction difficulty. Conversely, our approach requires only a single-step training process to train the entire network jointly and does not depend on external pre-trained SR networks for classifying the image patches regarding their reconstruction difficulties. Furthermore, it is worth noting that while ClassSR [20]’s approach involves the classification of image patches, our methodology encompasses the classification of each and every pixel within an image. This approach capitalizes on the entire spectrum of complexity and difficulty variations present within different image regions, consequently enabling its effectiveness in accommodating a wider range of diverse scenarios.

Mixture of Experts. As the demand for computational efficiency increases, MoE has emerged as a promising strategy. Its efficiency has led to its adoption across various domains, including natural language processing [13, 33], computer vision [31], and multimodal applications [27]. Despite its potential, MoE has not been widely adopted in SR tasks. Approaches resembling MoE, such as [20, 41], enhanced the performance of SR networks by employing multiple experts specialized in specific difficulty levels of patches. However, these approaches are limited to operating exclusively on a fixed scale factor. Furthermore, there is a noticeable absence of research dedicated to fully exploiting the potential of MoE in arbitrary-scale SR. Our work pioneers the utilization of MoE to tackle the computational complexity challenges inherent in arbitrary-scale SR, arising from its distinctive architectural characteristics.

3. Proposed Method

3.1. INR-Based SR

INR-based SR networks such as LIIF [9] and LTE [21] extract the input image’s INR z , using conventional SR networks such as EDSR [23], RDN [47], and SwinIR [22] as

their encoders. This process can formally be expressed as

$$z = E_\theta(I_{LR}), \quad (1)$$

where a LR input image $I_{LR} \in \mathbb{R}^{H \times W \times 3}$ is processed by E_θ , an encoder parameterized by θ , creating the INR $z \in \mathbb{R}^{H \times W \times D}$ which contains the information necessary to upscale I_{LR} . For each input pixel i , there is a corresponding INR $z_i \in \mathbb{R}^D$.

To predict the RGB value of the output pixel q , a matching input pixel k has to be found. Let us denote the center coordinate of pixel q and k as x_q and x_k , respectively. These coordinates are relative to the image size, therefore the domain of x_q and x_k are equal (e.g. $0 \leq x_q, x_k \leq 1$). Within the relative coordinate space, an input pixel k is chosen as the matching pixel for q which has the closest Euclidean distance between x_q and x_k among all input pixels.

Finally, a decoder takes the representation vector z_k and the relative coordinate $x_q - x_k$ to predict the final RGB value s_q of the output pixel q :

$$s_q = f_\phi(z_k, x_q - x_k), \quad (2)$$

where f_ϕ denotes the decoder parameterized by ϕ .

3.2. MoEISR

INR-based SR models are successful in that a single decoder f_ϕ can super-resolve images with arbitrary scale just by changing the query positions x_q . However, the computational demand becomes excessive as the decoder f_ϕ needs to be queried individually for predicting each output pixel q . Since the number of queries is difficult to reduce in INR-based SR approaches, we explored a new way to lighten the decoding function to mitigate the complexity. Our overall network architecture is described in Fig. 2.

Inspired by ClassSR [20], which employed distinct networks for image patches of varying complexities, our approach utilizes a set of experts with diverse capacities by considering the reconstruction difficulty of each input pixel. Instead of having a single resource-intensive decoder f_ϕ ,

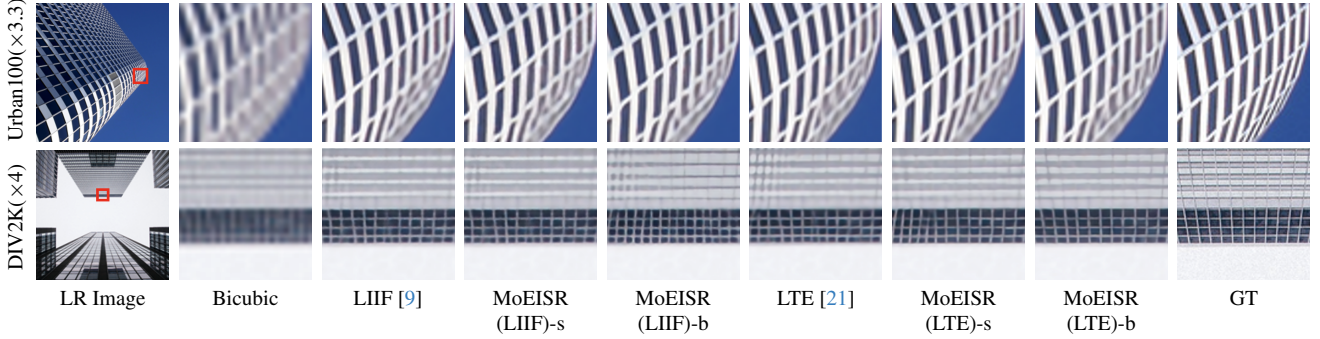


Figure 3. **In-scale qualitative comparison between MoEISR and the backbone models.** RDN [47] is used as an encoder for all methods.

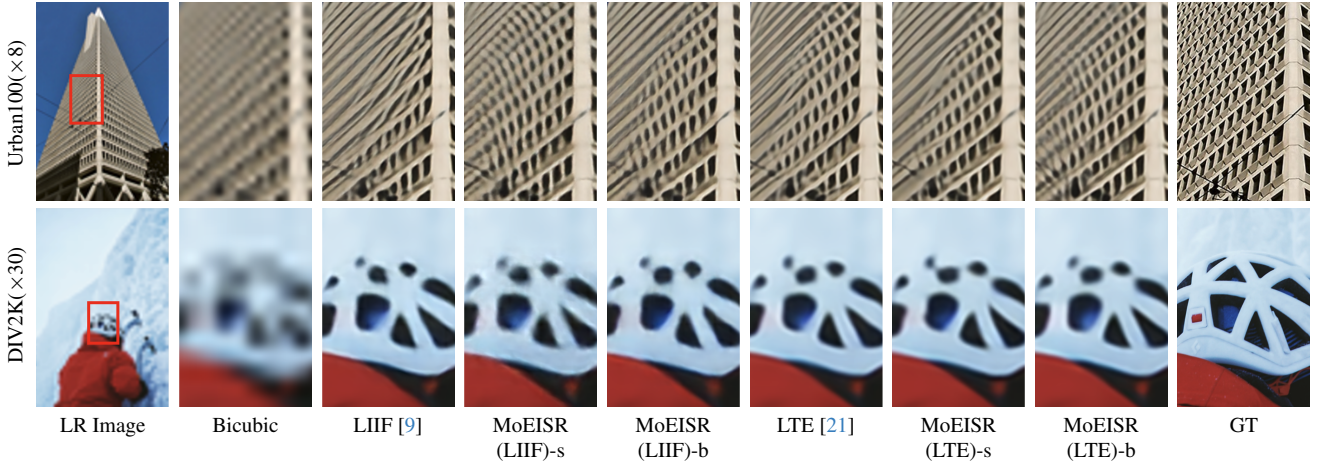


Figure 4. **Out-of-scale qualitative comparison between MoEISR and the backbone models.** RDN [47] is used as an encoder for all methods.

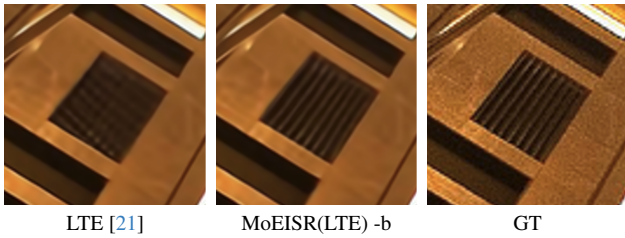


Figure 5. **Qualitative comparison between MoEISR(LTE) -b and LTE [21].** RDN [47] is used as an encoder.

our method uses a set of decoders $f_{\phi_1}^1, f_{\phi_2}^2, \dots, f_{\phi_J}^J$ with varying depths.

Among J decoders, a mapper M_ω selects the most suitable expert for each input pixel. It generates an expert map $D \in \mathbb{R}^{H \times W \times J}$ using the INR z :

$$D = M_\omega(z). \quad (3)$$

One can observe that classification is done on latent space instead of input space, unlike ClassSR [20]. We hypothesized that fast yet accurate pixel-wise classification could be done in latent space since representation for each



Figure 6. **Qualitative comparison between MoEISR(LIIF) -b and LIIF [9].** RDN [47] is used as an encoder.

input pixel z_k contains enough information to upscale the pixel, including its complexity. Our experiments show that the resulting expert map from D is highly correlated with local complexity (Fig. 1), influencing the performance of our model.

Using the classification result from the mapper, each output pixel q which corresponds to input pixel k is then processed by the most suitable expert. This expert is selected based on having the highest score within the score vector $D_k \in \mathbb{R}^J$ of the input pixel k , which describes the probability of the expert being selected for the pixel’s reconstruction.

Method	In-scale			Out-of-scale				
	×2	×3	×4	×6	×12	×18	×24	×30
Bicubic	31.01	28.22	26.66	24.82	22.27	21.00	20.19	19.59
EDSR-LIIF [9]	34.67	30.96	29.00	26.75	23.71	22.17	21.18	20.48
EDSR-MoEISR(LIIF) -s	34.60	30.91	28.96	26.70	23.66	22.13	21.14	20.45
EDSR-MoEISR(LIIF) -b	34.66	30.98	29.01	26.76	23.71	22.17	21.18	20.49
EDSR-LTE [21]	34.72	31.02	29.04	26.81	23.78	22.23	21.24	20.53
EDSR-MoEISR(LTE) -s	34.71	31.01	29.04	26.80	23.76	22.23	21.23	20.53
EDSR-MoEISR(LTE) -b	34.72	31.01	29.05	26.80	23.77	22.23	21.24	20.53
RDN-LIIF [9]	34.99	31.26	29.27	26.99	23.89	22.34	21.31	20.59
RDN-MoEISR(LIIF) -s	34.95	31.24	29.26	26.96	23.85	22.30	21.27	20.55
RDN-MoEISR(LIIF) -b	34.99	31.28	29.29	27.00	23.90	22.35	21.31	20.59
RDN-LTE [21]	35.04	31.32	29.33	27.04	23.95	22.40	21.36	20.64
RDN-MoEISR(LTE) -s	35.03	31.32	29.33	27.04	23.95	22.40	21.37	20.64
RDN-MoEISR(LTE) -b	35.05	31.33	29.33	27.05	23.96	22.40	21.37	20.64
SwinIR-LIIF [21]	35.17	31.46	29.46	27.15	24.02	22.43	21.40	20.67
SwinIR-MoEISR(LIIF) -s	35.20	31.48	29.48	27.17	24.05	22.48	21.45	20.71
SwinIR-MoEISR(LIIF) -b	35.22	31.49	29.49	27.18	24.07	22.48	21.46	20.72
SwinIR-LTE [21]	35.24	31.50	29.51	27.20	24.09	22.50	21.47	20.73
SwinIR-MoEISR(LTE) -s	35.25	31.51	29.52	27.20	24.08	22.50	21.47	20.73
SwinIR-MoEISR(LTE) -b	35.24	31.50	29.51	27.20	24.08	22.50	21.47	20.72

Table 1. Quantitative comparison on DIV2K validation set [1]. **Bold** indicates the best PSNR among the backbone network and its MoEISR variant.

tion. The process can be described as follows:

$$s_q = f_{\phi_j}^j(z_k, x_q - x_k),$$

where $j = \operatorname{argmax}_{i \in \{1, \dots, J\}} D_{ki}$, (4)

and where D_{ki} denotes i th element of D_k . Although using the argmax operation for expert selection is the key to achieving speed-up at test-time, this operation is not differentiable, thereby obstructing gradient flow during training. To address the issue, we modify Eq. 4 to the weighted sum of decoders during training, as follows:

$$s_q = \sum_{j=1}^J g(D_k)_j \times f_{\phi_j}^j(z_k, x_q - x_k),$$
 (5)

where g denotes the Gumbel-softmax function [17, 24]. To be specific, we adopt Gumbel-softmax [17, 24] instead of softmax to prevent the mapper from being biased towards its decisions in the early stage of training. The utilization of Gumbel-softmax [17, 24] helps prevent such overfitting by introducing noise and is proven to be effective [34, 39]. This approach offers enhanced training flexibility, mitigating the risk of the network getting trapped in local optima. Notably, we maintain Eq. 4 in its original form during inference.

Our MoEISR framework is model-agnostic and compatible with any SR networks based on INR. It is also feasible to integrate various techniques, including cell decoding and feature unfolding from LIIF [9], as well as scale-dependent phase estimation from LTE [21]. This flexibility allows for the incorporation of various enhancements to tailor MoEISR to specific tasks and requirements.

3.3. Loss Functions

Our loss function has two distinct terms, L_1 , the reconstruction loss, and L_b , the balance loss. L_1 serves to gauge the quality of reconstruction, which is commonly used in SR tasks. L_b loss, on the other hand, ensures that the mapper assigns pixels to capacity-varying experts in a balanced manner. This dual loss contributes to the stable training of the network. The overall loss function can be described as:

$$L = \alpha L_1 + \beta L_b, \quad (6)$$

where α and β represent the weights balancing two loss terms.

The balance loss L_b plays a critical role in MoEISR. Without L_b , the mapper might assign all input pixels to the deepest decoder, rather than utilizing all available experts in a balanced manner. The balance loss helps ensure a more balanced distribution of experts among pixels, promoting a more efficient utilization of the model’s capacity. The formulation of the balance loss can be described as:

$$L_b = \sum_{j=1}^J \left| w_j \sum_{k=1}^K D_{kj} - \frac{K}{J} \right|, \quad (7)$$

where J denotes the number of experts and K represents the number of input pixels. The balance loss is a modified version of average loss used in ClassSR [20], further incorporating hyperparameters w_j . With $w_j = 1$ for all j , it penalizes the mapper if its expert assignment is not uniform, ensuring $\mathbb{E}[D_k] \simeq \frac{1}{J}(1 \dots 1)^T$ for a random input pixel k . One can regulate the ratio of experts chosen by changing the value of w_j . This would be especially useful when the model is deployed to devices with varying computational capacities.

3.4. Training Strategy

For training, we first downscale the input image to a random scale from $1 \times$ to $4 \times$ so that the network can learn to upscale the image in an arbitrary scale. Similar to the evaluation methodologies employed in LIIF [9] and LTE [21], our network is also evaluated at scales like $8 \times$ and $32 \times$ that have not been encountered during its training phase with the aim of demonstrating the network’s capacity for generalization. During the training phase, we aggregate the outputs of individual experts, weighted by probabilities derived from Gumbel-softmax [17, 24], indicating the suitability of each decoder for an output pixel. In the testing phase, we simplify the methodology by straightforwardly selecting the expert with the highest probability, leading to the computation of the final output. This streamlined process achieves image reconstruction with significantly reduced computational load.

Method	Set5 [4]				Set14 [45]				B100 [25]				Urban100 [16]							
	In-scale			Out-of-scale	In-scale			Out-of-scale	In-scale			Out-of-scale	In-scale			Out-of-scale				
	×2	×3	×4		×2	×3	×4		×2	×3	×4		×2	×3	×4					
RDN [47]	38.24	34.71	32.47	-	34.01	30.57	28.81	-	-	32.34	29.26	27.72	-	-	32.89	28.80	26.61	-	-	
RDN-LIIF [9]	38.17	34.68	32.50	29.15	27.14	33.97	30.53	28.80	26.64	25.15	32.32	29.26	27.74	25.98	24.91	32.87	28.82	26.68	24.20	22.79
RDN-MoEISR(LIIF) -s	38.17	34.66	32.49	29.20	27.13	33.98	30.52	28.82	26.61	25.09	32.32	29.25	27.74	25.97	24.91	32.82	28.80	26.65	24.15	22.76
RDN-MoEISR(LIIF) -b	38.19	34.69	32.46	29.27	27.25	33.99	30.56	28.82	26.66	25.20	32.33	29.28	27.75	25.98	24.93	32.93	28.90	26.74	24.24	22.84
RDN [47]	38.24	34.71	32.47	-	-	34.01	30.57	28.81	-	-	32.34	29.26	27.72	-	-	32.89	28.80	26.61	-	-
RDN-LTE [21]	38.23	34.72	32.61	29.32	27.26	34.09	30.58	28.88	26.71	25.16	32.36	29.30	27.77	26.01	24.95	33.04	28.97	26.81	24.28	22.88
RDN-MoEISR(LTE) -s	38.21	34.70	32.49	29.24	27.24	33.99	30.59	28.86	26.69	25.18	32.36	29.30	27.77	26.00	24.94	33.02	28.94	26.79	24.25	22.86
RDN-MoEISR(LTE) -b	38.25	34.78	32.53	29.24	27.20	34.10	30.58	28.86	26.71	25.22	32.37	29.30	27.78	26.01	24.95	33.06	28.98	26.83	24.31	22.89
SwinIR [22]	38.35	34.89	32.72	-	-	34.14	30.77	28.94	-	-	32.44	29.37	27.83	-	-	33.40	29.29	27.07	-	-
SwinIR-LIIF [21]	38.28	34.87	32.73	29.46	27.36	34.14	30.75	28.98	26.82	25.34	32.39	29.34	27.84	26.07	25.01	33.36	29.33	27.15	24.59	23.14
SwinIR-MoEISR(LIIF) -s	38.30	34.85	32.72	29.45	27.34	34.25	30.77	29.01	26.82	25.35	32.42	29.36	27.84	26.07	25.01	33.41	29.40	27.19	24.58	23.13
SwinIR-MoEISR(LIIF) -b	38.30	34.85	32.77	29.48	27.39	34.24	30.78	29.02	26.87	25.36	32.43	29.37	27.85	26.08	25.02	33.48	29.42	27.22	24.62	23.16
SwinIR-LTE [21]	38.33	34.89	32.81	29.50	27.35	34.25	30.80	29.06	26.86	25.42	32.44	29.39	27.86	26.09	25.03	33.50	29.41	27.24	24.62	23.17
SwinIR-MoEISR(LTE) -s	38.35	34.90	32.78	29.53	27.42	34.27	30.80	29.03	26.87	25.40	32.45	29.39	27.87	26.09	25.03	33.52	29.45	27.25	24.66	23.18
SwinIR-MoEISR(LTE) -b	38.34	34.88	32.79	29.47	27.37	34.24	30.77	29.03	26.81	25.39	32.44	29.38	27.86	26.09	25.03	33.49	29.40	27.24	24.63	23.18

Table 2. Quantitative comparison on various benchmark datasets. **Bold** indicates the best PSNR among the backbone network and its MoEISR variant.

Method	In-scale						Out-of-scale									
	×2	%	×3	%	×4	%	×6	%	×12	%	×18	%	×24	%	×30	%
EDSR-LIIF [9]	1.55TF	100%	3.15TF	100%	5.38TF	100%	11.75TF	100%	46.14TF	100%	103.46TF	100%	183.72TF	100%	286.90TF	100%
EDSR-MoEISR(LIIF) -b	1.15TF	74.10%	2.23TF	71.00%	3.75TF	69.73%	8.08TF	68.78%	31.45TF	68.16%	70.40TF	68.04%	124.96TF	68.02%	195.06TF	67.99%
EDSR-MoEISR(LIIF) -s	0.62TF	39.88%	1.04TF	32.95%	1.62TF	30.15%	3.29TF	28.01%	12.30TF	26.66%	27.31TF	26.40%	48.34TF	26.31%	75.37TF	26.27%
EDSR-LTE [21]	1.01TF	100%	1.92TF	100%	3.19TF	100%	6.82TF	100%	26.45TF	100%	59.17TF	100%	104.97TF	100%	163.85TF	100%
EDSR-MoEISR(LTE) -b	0.95TF	94.58%	1.79TF	93.22%	2.95TF	92.62%	6.29TF	92.14%	24.29TF	91.81%	54.29TF	91.76%	96.29TF	91.74%	150.30TF	91.73%
EDSR-MoEISR(LTE) -s	0.48TF	47.75%	0.72TF	37.78%	1.07TF	33.43%	2.04TF	29.91%	7.30TF	27.61%	16.08TF	27.17%	28.36TF	27.02%	44.16TF	26.95%
RDN-LIIF [9]	6.33TF	100%	7.92TF	100%	10.15TF	100%	16.52TF	100%	50.92TF	100%	108.24TF	100%	188.49TF	100%	291.68TF	100%
RDN-MoEISR(LIIF) -b	6.05TF	95.50%	7.27TF	91.82%	9.00TF	88.62%	13.91TF	84.22%	40.47TF	79.48%	84.73TF	78.28%	146.67TF	77.81%	226.35TF	77.60%
RDN-MoEISR(LIIF) -s	5.40TF	85.37%	5.83TF	73.61%	6.43TF	63.34%	8.14TF	49.27%	17.38TF	34.13%	32.77TF	30.28%	54.32TF	28.82%	82.02TF	28.12%
RDN-LTE [21]	5.78TF	100%	6.69TF	100%	7.96TF	100%	11.60TF	100%	31.23TF	100%	63.94TF	100%	109.74TF	100%	168.63TF	100%
RDN-MoEISR(LTE) -b	5.75TF	99.36%	6.60TF	98.65%	7.80TF	97.93%	11.22TF	96.74%	29.70TF	95.10%	60.49TF	94.61%	103.60TF	94.40%	159.03TF	94.31%
RDN-MoEISR(LTE) -s	5.29TF	91.53%	5.58TF	83.42%	5.99TF	75.18%	7.14TF	61.60%	13.39TF	42.88%	23.81TF	37.23%	38.38TF	34.98%	57.13TF	33.88%
SwinIR-LIIF [21]	1.30TF	100%	2.89TF	100%	5.12TF	100%	11.49TF	100%	45.89TF	100%	103.21TF	100%	183.47TF	100%	286.65TF	100%
SwinIR-MoEISR(LIIF) -b	0.98TF	74.91%	2.15TF	74.33%	3.80TF	74.11%	8.50TF	74.00%	33.92TF	73.92%	76.25TF	73.88%	135.54TF	73.88%	211.52TF	73.79%
SwinIR-MoEISR(LIIF) -s	0.38TF	29.20%	0.81TF	28.13%	1.42TF	27.75%	3.16TF	27.47%	12.52TF	27.29%	28.13TF	27.26%	50.02TF	27.26%	78.03TF	27.22%
SwinIR-LTE [21]	0.75TF	100%	1.66TF	100%	2.94TF	100%	6.57TF	100%	26.20TF	100%	58.91TF	100%	104.71TF	100%	163.60TF	100%
SwinIR-MoEISR(LTE) -b	0.77TF	95.91%	1.56TF	93.70%	2.73TF	92.84%	6.06TF	92.27%	24.10TF	91.97%	54.10TF	91.83%	96.13TF	91.80%	150.19TF	91.80%
SwinIR-MoEISR(LTE) -s	0.28TF	37.61%	0.57TF	34.16%	0.97TF	32.90%	2.10TF	32.00%	8.24TF	31.45%	18.45TF	31.32%	32.78TF	31.31%	51.19TF	31.29%

Table 3. Quantitative comparison on Set14 validation set [45]. **Bold** indicates the least FLOPs required among the backbone network and its MoEISR variant.

4. Experiment

The code implementation of MoEISR will be available upon acceptance. More details and additional results can be found in our supplementary material.

Datasets. Our approach employs the identical dataset as our backbone models: LIIF [9] and LTE [21]. Both of these models are trained on the DIV2K dataset from the NTIRE 2017 Challenge [1]. Subsequently, our evaluation procedure is based on several benchmark datasets, including the DIV2K validation set [1], Set5 [4], Set14 [45], B100 [25], and Urban100 [16].

Implementation Details. Since our research is model-agnostic and generally applicable to conventional INR-based arbitrary-scale SR networks, we adopt a consistent approach with the implementations of our backbone models. Specifically, we configure our network to process 48×48 patches as input data. For the baseline encoders, we choose EDSR [23], RDN [47], and SwinIR [22]. For MoEISR employing LIIF [9] as the backbone, we employ 4 capacity-varying experts, while for the LTE [21] version,

3 capacity-varying experts are utilized, each mirroring the depth of its original decoder as the heaviest expert. We use the conventional L1 loss [20] and the balance loss with $\alpha = 3000$ and $\beta = 1$ with the Adam [19] optimizer. The learning rate is set equivalent to that of the backbone network. For the mapper, we use a 5-layer convolutional neural network and a Gumbel-softmax [17, 24] with temperature hyperparameter $\tau = 1$ for normalization by default.

4.1. Evaluation

Quantitative Results. Tab. 1 describes a quantitative analysis between the MoEISR approach based on LIIF [9] and LTE [21], using EDSR [23], RDN [47], and SwinIR [22] as encoder. MoEISR -b is our baseline model, which incorporates experts with 256 hidden dimensions while varying the depth in the decoder and MoEISR -s employs experts with 128 hidden dimensions with varying depths, notably decreasing computational complexity. Tab. 1 clearly indicates that the MoEISR -b models exhibit impressive performance, attaining comparable or even superior PSNR values to its backbone network across various

Method	In-scale				Out-of-scale					
	×2	FLOPs	×3	FLOPs	×4	FLOPs	×6	FLOPs	×8	FLOPs
RDN-MoEISR(LIIF) -b	32.93	5.09TFLOPs	28.90	2.74TFLOPs	26.74	1.92TFLOPs	24.24	1.34TFLOPs	22.84	1.14TFLOPs
RDN-MoEISR(LIIF) -s	32.82	4.55TFLOPs	28.80	2.18TFLOPs	26.65	1.36TFLOPs	24.15	0.76TFLOPs	22.76	0.56TFLOPs
LIIF -5layer [9]	32.87	5.33TFLOPs	28.82	2.96TFLOPs	26.68	2.13TFLOPs	24.20	1.53TFLOPs	22.79	1.34TFLOPs
LIIF -4layer	32.83	5.13TFLOPs	28.80	2.76TFLOPs	26.64	1.93TFLOPs	24.15	1.33TFLOPs	22.75	1.13TFLOPs
LIIF -3layer	32.85	4.92TFLOPs	28.84	2.55TFLOPs	26.67	1.73TFLOPs	24.13	1.13TFLOPs	22.71	0.93TFLOPs
LIIF -2layer	32.48	4.72TFLOPs	28.44	2.35TFLOPs	26.24	1.53TFLOPs	23.83	0.93TFLOPs	22.49	0.73TFLOPs

Table 4. **Ablation study on MoEISR and LIIF [9] with different decoder depths.** -5layer, -4layer, -3layer and -2layer refers to the decoder depth. **Red** and **blue** indicate the best PSNR and least FLOPs, respectively.

scenarios. Interestingly, MoEISR -s also demonstrates competitive reconstruction capabilities, occasionally even outperforming the original backbone network. In Tab. 2, we further conduct a comparative analysis on MoEISR based on LIIF [9] and LTE [21], using RDN [47] and SwinIR [22] as encoders, across various benchmark datasets. As already shown in Tab. 1, MoEISR -b outperforms its respective backbone networks in the majority of cases and MoEISR -s also demonstrates impressive performance, occasionally even surpassing MoEISR -b.

Tab. 3 provides a detailed description of the FLOPs required to upscale HR images from the Set14 dataset [45] to various scales. As expected, MoEISR, with its adoption of layer-varying experts, consistently yields lower FLOPs for both versions of MoEISR compared to their respective backbone networks. Moreover, the FLOPs disparity becomes more pronounced with an increase in the upscaling factor. A noteworthy point that deserves attention is that MoEISR -s, which has demonstrated its competitive upscaling ability in Tab. 1 and Tab. 2, requires significantly lower FLOPs than the original model. SwinIR-MoEISR(LTE) -s, operating at a scaling factor of 2, requires only 37.61% of the FLOPs compared to the original SwinIR-LTE [9] model. Furthermore, EDSR-MoEISR(LIIF) -s with a scaling factor of 30 requires even less FLOPs, and it requires only 26.27% of the FLOPs compared to EDSR-LIIF [9].

Qualitative Results. Fig. 3 and Fig. 4 provide a comprehensive qualitative comparison on MoEISR and its associated backbone models under in-scale and out-of-scale upscaling factors. These models are trained with RDN [47] as the encoder. It is readily apparent that MoEISR outperforms its backbone models in the reconstruction of finer details, regardless of whether the context is in-scale or out-of-scale. For instance, the MoEISR(LTE) -b model notably excels in reconstructing square-shaped windows, demonstrating superior performance compared to the LTE [21] model on both DIV2K [1] and Urban100 [16] datasets. Furthermore, as illustrated in Fig. 5, our model demonstrates a high degree of accuracy in reconstructing the window with diagonal patterns, in contrast to the window reconstructed by LTE [21]. Fig. 6 visually highlights a noticeable disparity in reconstruction quality between LIIF [9] and MoEISR(LIIF) -b. Where LIIF [9] exhibits difficulties in upscaling letters

accurately, our model adeptly reconstructs the letters with minimal deformation in shape. The observed discrepancy in the representation of finer details is due to the effective use of the mapper within our model. The mapper enables our model to capture the intricate relationships between individual pixels, thereby enhancing its ability to reconstruct detailed images.

4.2. Ablation Study

In this section, we perform a comprehensive ablation study of each component within MoEISR and evaluate its impact on the overall performance.

Fixed Decoder. To assess the effectiveness of MoEISR, we compare our models to LIIF [9] with various decoder configurations. RDN [47] is used as an encoder for all models and is evaluated with the urban100 dataset [16]. Tab. 4 describes the differences in PSNR and FLOPs across varying model architectures and the notations -5layer, -4layer, -3layer, and -2layer denote the respective number of convolutional layers within the decoder. The acquired outcomes undeniably demonstrate the efficacy of MoEISR. Specifically, MoEISR(LIIF) -b consistently achieves the highest PSNR while maintaining a comparable level of FLOPs as that of LIIF-4layer, which yields about 0.1db lower PSNR than MoEISR(LIIF) -b. Moreover, it is worth noting that MoEISR(LIIF) -s consistently demands the least amount of FLOPs while still achieving competitive PSNR values, similar to those of LIIF -4layer, which necessitates significantly larger FLOPs.

Mapper Depth. The mapper module, which is responsible for determining the appropriate expert for restoring each output pixel, consists of five convolutional layers. Inspired by APE [41], which employs a single-layered regressor, we explore a modified version of MoEISR. This variant incorporates a notably lighter mapper module, comprising only a single convolutional layer. Tab. 5 provides a clear representation of the performance of MoEISR with varying mapper depths. It is worth noting that the utilization of a 1-layered mapper module results in a reduction of FLOPs, but there is also a corresponding decrease in both PSNR and SSIM. Fig. 7 visually depicts the expert maps generated by the mapper modules with varying depths. It is evident that the 5-layered mapper produces a more intricate expert map

Method	PSNR	SSIM	FLOPs
MoEISR(LIIF) -b	29.2909	0.8273	6.84TFLOPs
MoEISR(LIIF) -b -m1	29.1685	0.8251	5.61TFLOPs

Table 5. **Ablation study on the mapper depth of MoEISR.** All methods are evaluated on $4\times$ bicubic downsampled DIV2K validation dataset [1]. -m1 refers to MoEISR with a 1-layered mapper.

Method	PSNR	SSIM	FLOPs
MoEISR(LIIF) -b	29.2909	0.8273	6.84TFLOPs
MoEISR(LIIF) -b - τ 3	29.2099	0.8264	6.43TFLOPs
MoEISR(LIIF) -b - τ 5	29.1811	0.8260	6.39TFLOPs

Table 6. **Ablation study on the temperature hyperparameter of MoEISR.** All methods are evaluated on $4\times$ bicubic downsampled DIV2K validation dataset [1]. τ 3 and τ 5 refers to MoEISR with temperature hyperparameter $\tau = 3$ and $\tau = 5$.

compared to the 1-layered mapper. For instance, 5-layered mapper adeptly captures the fine details of the grass adjacent to the fur, whereas 1-layered mapper struggles to assign the appropriate decoders to the area. Nevertheless, since our mapper is executed only once like the encoder, the use of the 5-layer mapper does not significantly impact on the overall FLOPs during the $4\times$ high-resolution image reconstruction process.

Temperature Hyperparameter. In our approach, we employ Gumbel-softmax [17, 24] with temperature hyperparameter $\tau = 1$. This temperature hyperparameter plays a key role in the assignment of experts to the output pixels and has a substantial impact on the efficacy of MoEISR. Fig. 8 shows different expert maps generated with different temperature hyperparameters. In MoEISR, we do not force the mapper to assign experts equally, therefore achieving a balanced trade-off between performance and efficiency. This behavior is accomplished by configuring the hyperparameter τ to a value of 1, thus intensifying the probability discrepancies among different experts. As described in Tab. 6, when the hyperparameter τ is set to 3, our Mapper yields a lower PSNR and SSIM values with reduced FLOPs, and this effect becomes more pronounced as the value of τ increases.

Controllable Mapper. We conduct additional experiments to explore the extent to which we can control the trade-off between the speed and quality of the model. In Eq. (7), hyperparameter w_i is multiplied to control the assignment of experts to the output pixels. By simply altering the values of w_i during the training phase, we can effectively determine the frequency of assignments for each expert. The visualization of expert map with varying w_i can be found in the supplementary materials. When w_4 is set to 2, the mapper module allocates the 4-th expert (5-layered expert) less frequently, while setting w_1 to 2 leads to reduced usage of the 1-st expert (2-layered expert). This control over expert allocation allows us to balance the com-

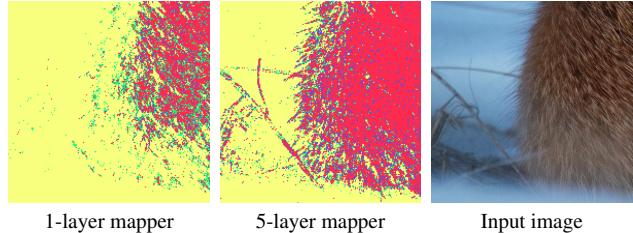


Figure 7. **Ablation study on the mapper depths of MoEISR.** Expert map (experts chosen with the highest probability) of 1-layer mapper (left), 5-layer mapper (middle) and input image (right). Yellow, green, blue, and red pixels denote different layered experts.

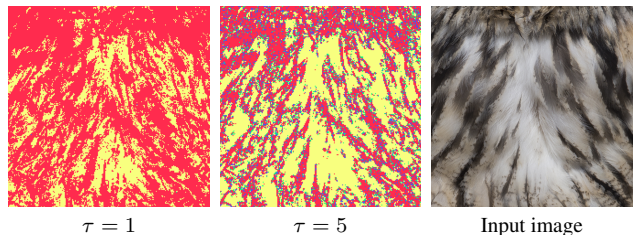


Figure 8. **Ablation study on the temperature hyperparameter of MoEISR.** Expert map (experts chosen with the highest probability) with $\tau = 1$ (left), $\tau = 5$ (middle) and input image (right). Yellow, green, blue and red pixels denote different layered experts.

putational load and restoration quality effectively.

5. Conclusion

In this paper, we present MoEISR, a novel approach that achieves the dual goal of significantly reducing computational requirements while maintaining competitive SR image quality. One of the key advantages of our method is its versatility, as it can be smoothly integrated into any INR-based arbitrary-scale SR framework. MoEISR consists of three core components: an encoder, a mapper, and a set of experts. The encoder is responsible for extracting INR from the input image, while the mapper generates an expert map that assigns the most suitable expert to each output pixel regarding its reconstruction difficulty. The central concept behind MoEISR is the use of a mapper module in conjunction with a set of experts with varying depths, allowing each pixel to be reconstructed with the most suitable expert. By using multiple experts, as opposed to a single computationally-heavy decoder, each expert specializes in reconstructing different regions within the image, ultimately resulting in high-quality SR images with a reduced computational load. Extensive experiments presented in the paper demonstrate the ability of our MoEISR to improve the quality of existing INR-based arbitrary-scale SR networks, while simultaneously significantly reducing computational requirements.

References

- [1] Eirikur Agustsson and Radu Timofte. Ntire 2017 challenge on single image super-resolution: Dataset and study. In *Proceedings of the IEEE/CVF Conference on Computer Vision and Pattern Recognition Workshops (CVPRW)*, 2017. 5, 6, 7, 8
- [2] Ivan Anokhin, Kirill Demochkin, Taras Khakhulin, Gleb Sterkin, Victor Lempitsky, and Denis Korzhenkov. Image generators with conditionally-independent pixel synthesis. In *Proceedings of the IEEE/CVF Conference on Computer Vision and Pattern Recognition (CVPR)*, 2021. 2
- [3] Matan Atzmon and Yaron Lipman. Sal: Sign agnostic learning of shapes from raw data. In *IEEE/CVF Conference on Computer Vision and Pattern Recognition (CVPR)*, 2020. 2
- [4] Marco Bevilacqua, Aline Roumy, Christine M. Guillemot, and Marie-Line Alberi-Morel. Low-complexity single-image super-resolution based on nonnegative neighbor embedding. In *British Machine Vision Conference*, 2012. 6
- [5] Jiezhong Cao, Qin Wang, Yongqin Xian, Yawei Li, Bingbing Ni, Zhiming Pi, Kai Zhang, Yulun Zhang, Radu Timofte, and Luc Van Gool. Ciaosr: Continuous implicit attention-inattention network for arbitrary-scale image super-resolution. In *Proceedings of the IEEE/CVF Conference on Computer Vision and Pattern Recognition (CVPR)*, 2023. 1, 2
- [6] Hanting Chen, Yunhe Wang, Tianyu Guo, Chang Xu, Yiping Deng, Zhenhua Liu, Siwei Ma, Chunjing Xu, Chao Xu, and Wen Gao. Pre-trained image processing transformer. In *Proceedings of the IEEE/CVF Conference on Computer Vision and Pattern Recognition (CVPR)*, 2021. 1, 2
- [7] Hao-Wei Chen, Yu-Syuan Xu, Min-Fong Hong, Yi-Min Tsai, Hsien-Kai Kuo, and Chun-Yi Lee. Cascaded local implicit transformer for arbitrary-scale super-resolution. In *Proceedings of the IEEE/CVF Conference on Computer Vision and Pattern Recognition (CVPR)*, 2023. 1, 2
- [8] Xiangyu Chen, Xintao Wang, Jiantao Zhou, Yu Qiao, and Chao Dong. Activating more pixels in image super-resolution transformer. In *Proceedings of the IEEE/CVF Conference on Computer Vision and Pattern Recognition (CVPR)*, 2023. 1, 2
- [9] Yinbo Chen, Sifei Liu, and Xiaolong Wang. Learning continuous image representation with local implicit image function. In *Proceedings of the IEEE/CVF Conference on Computer Vision and Pattern Recognition (CVPR)*, 2021. 1, 2, 3, 4, 5, 6, 7
- [10] Zhiqin Chen and Hao Zhang. Learning implicit fields for generative shape modeling. In *Proceedings of the IEEE/CVF Conference on Computer Vision and Pattern Recognition (CVPR)*, 2019. 2
- [11] Zeyuan Chen, Yinbo Chen, Jingwen Liu, Xingqian Xu, Vidit Goel, Zhangyang Wang, Humphrey Shi, and Xiaolong Wang. Videoinr: Learning video implicit neural representation for continuous space-time super-resolution. In *Proceedings of the IEEE/CVF Conference on Computer Vision and Pattern Recognition (CVPR)*, 2022. 2
- [12] Chao Dong, Chen Change Loy, Kaiming He, and Xiaoou Tang. Image super-resolution using deep convolutional networks. *IEEE Transactions on Pattern Analysis and Machine Intelligence*, 38(2):295–307, 2016. 2
- [13] William Fedus, Barret Zoph, and Noam Shazeer. Switch transformers: Scaling to trillion parameter models with simple and efficient sparsity. *The Journal of Machine Learning Research*, 23(1):5232–5270, 2022. 2, 3
- [14] Stephan J Garbin, Marek Kowalski, Matthew Johnson, Jamie Shotton, and Julien Valentin. Fastnerf: High-fidelity neural rendering at 200fps. *arXiv preprint arXiv:2103.10380*, 2021. 2
- [15] Xuecai Hu, Haoyuan Mu, Xiangyu Zhang, Zilei Wang, Tieniu Tan, and Jian Sun. Meta-sr: A magnification-arbitrary network for super-resolution. In *Proceedings of the IEEE/CVF Conference on Computer Vision and Pattern Recognition (CVPR)*, 2019. 1, 2
- [16] Jia-Bin Huang, Abhishek Singh, and Narendra Ahuja. Single image super-resolution from transformed self-exemplars. In *Proceedings of the IEEE/CVF Conference on Computer Vision and Pattern Recognition (CVPR)*, 2015. 6, 7
- [17] Eric Jang, Shixiang Gu, and Ben Poole. Categorical reparameterization with gumbel-softmax. In *International Conference on Learning Representations (ICLR)*, 2017. 5, 6, 8
- [18] Chiyu “Max” Jiang, Avneesh Sud, Ameesh Makadia, Jingwei Huang, Matthias Niessner, and Thomas Funkhouser. Local implicit grid representations for 3d scenes. In *Proceedings of the IEEE/CVF Conference on Computer Vision and Pattern Recognition (CVPR)*, 2020. 2
- [19] Diederik Kingma and Jimmy Ba. Adam: A method for stochastic optimization. In *International Conference on Learning Representations (ICLR)*, San Diego, CA, USA, 2015. 6
- [20] Xiangtao Kong, Hengyuan Zhao, Yu Qiao, and Chao Dong. Classsr: A general framework to accelerate super-resolution networks by data characteristic. In *Proceedings of the IEEE/CVF Conference on Computer Vision and Pattern Recognition (CVPR)*, 2021. 1, 2, 3, 4, 5, 6, 7
- [21] Jaewon Lee and Kyong Hwan Jin. Local texture estimator for implicit representation function. In *Proceedings of the IEEE/CVF Conference on Computer Vision and Pattern Recognition (CVPR)*, 2022. 1, 2, 3, 4, 5, 6, 7
- [22] Jingyun Liang, Jiezhong Cao, Guolei Sun, Kai Zhang, Luc Van Gool, and Radu Timofte. Swinir: Image restoration using swin transformer. In *Proceedings of the IEEE/CVF International Conference on Computer Vision Workshops (ICCVW)*, 2021. 1, 2, 3, 6, 7
- [23] Bee Lim, Sanghyun Son, Heewon Kim, Seungjun Nah, and Kyoung Mu Lee. Enhanced deep residual networks for single image super-resolution. In *Proceedings of the IEEE/CVF Conference on Computer Vision and Pattern Recognition Workshops (CVPRW)*, 2017. 1, 2, 3, 6
- [24] Chris J. Maddison, Andriy Mnih, and Yee Whye Teh. The concrete distribution: A continuous relaxation of discrete random variables. In *International Conference on Learning Representations*, 2017. 5, 6, 8
- [25] D. Martin, C. Fowlkes, D. Tal, and J. Malik. A database of human segmented natural images and its application to evaluating segmentation algorithms and measuring ecologi-

- cal statistics. In *Proceedings of the IEEE/CVF International Conference on Computer Vision (ICCV)*, 2001. 6
- [26] Ben Mildenhall, Pratul P. Srinivasan, Matthew Tancik, Jonathan T. Barron, Ravi Ramamoorthi, and Ren Ng. Nerf: Representing scenes as neural radiance fields for view synthesis. In *Proceedings of the European Conference on Computer Vision (ECCV)*, 2020. 2
- [27] Basil Mustafa, Carlos Riquelme, Joan Puigcerver, Rodolphe Jenatton, and Neil Houlsby. Multimodal contrastive learning with limoe: the language-image mixture of experts. *Advances in Neural Information Processing Systems*, 35:9564–9576, 2022. 2, 3
- [28] Michael Niemeyer, Lars Mescheder, Michael Oechsle, and Andreas Geiger. Differentiable volumetric rendering: Learning implicit 3d representations without 3d supervision. In *Proceedings of the IEEE/CVF Conference on Computer Vision and Pattern Recognition (CVPR)*, 2020. 2
- [29] Michael Oechsle, Lars Mescheder, Michael Niemeyer, Thilo Strauss, and Andreas Geiger. Texture fields: Learning texture representations in function space. In *Proceedings of the IEEE/CVF International Conference on Computer Vision (ICCV)*, 2019.
- [30] Christian Reiser, Songyou Peng, Yiyi Liao, and Andreas Geiger. Kilonerf: Speeding up neural radiance fields with thousands of tiny mlps. In *Proceedings of the IEEE/CVF International Conference on Computer Vision (ICCV)*, 2021. 2
- [31] Carlos Riquelme, Joan Puigcerver, Basil Mustafa, Maxim Neumann, Rodolphe Jenatton, André Susano Pinto, Daniel Keysers, and Neil Houlsby. Scaling vision with sparse mixture of experts. *Advances in Neural Information Processing Systems*, 34:8583–8595, 2021. 2, 3
- [32] Yaniv Romano, John R. Isidoro, and Peyman Milanfar. Rair: Rapid and accurate image super resolution. *IEEE Transactions on Computational Imaging*, 3:110–125, 2016. 2
- [33] Noam Shazeer, Azalia Mirhoseini, Krzysztof Maziarz, Andy Davis, Quoc Le, Geoffrey Hinton, and Jeff Dean. Outrageously large neural networks: The sparsely-gated mixture-of-experts layer. *arXiv preprint arXiv:1701.06538*, 2017. 3
- [34] Jiayi Shen, Xiantong Zhen, Marcel Worring, and Ling Shao. Variational multi-task learning with gumbel-softmax priors. In *Advances in Neural Information Processing Systems*, 2021. 5
- [35] Wenzhe Shi, Jose Caballero, Ferenc Huszar, Johannes Totz, Andrew P. Aitken, Rob Bishop, Daniel Rueckert, and Zehan Wang. Real-time single image and video super-resolution using an efficient sub-pixel convolutional neural network. In *Proceedings of the IEEE/CVF Conference on Computer Vision and Pattern Recognition (CVPR)*, 2016. 1
- [36] Vincent Sitzmann, Michael Zollhoefer, and Gordon Wetzstein. Scene representation networks: Continuous 3d-structure-aware neural scene representations. In *Advances in Neural Information Processing Systems*. Curran Associates, Inc., 2019. 2
- [37] Ivan Skorokhodov, Savva Ignatyev, and Mohamed Elhoseiny. Adversarial generation of continuous images. In *Proceedings of the IEEE/CVF Conference on Computer Vision and Pattern Recognition (CVPR)*, 2021. 2
- [38] Sanghyun Son and Kyoung Mu Lee. Srwarp: Generalized image super-resolution under arbitrary transformation. In *Proceedings of the IEEE/CVF Conference on Computer Vision and Pattern Recognition (CVPR)*, 2021. 1, 2
- [39] Ximeng Sun, Rameswar Panda, Rogerio Feris, and Kate Saenko. Adashare: Learning what to share for efficient deep multi-task learning. *Advances in Neural Information Processing Systems*, 33, 2020. 5
- [40] Longguang Wang, Yingqian Wang, Zaiping Lin, Jungang Yang, Wei An, and Yulan Guo. Learning a single network for scale-arbitrary super-resolution. In *Proceedings of the IEEE/CVF International Conference on Computer Vision (ICCV)*, 2021. 1, 2
- [41] Shizun Wang, Jiaming Liu, Kaixin Chen, Xiaoqi Li, Ming Lu, and Yandong Guo. Adaptive patch exiting for scalable single image super-resolution. In *Proceedings of the European Conference on Computer Vision (ECCV)*, 2022. 1, 3, 7
- [42] Xiaohang Wang, Xuanhong Chen, Bingbing Ni, Hang Wang, Zhengyan Tong, and Yutian Liu. Deep arbitrary-scale image super-resolution via scale-equivariance pursuit. In *Proceedings of the IEEE/CVF Conference on Computer Vision and Pattern Recognition (CVPR)*, 2023. 1, 2
- [43] Ke Yu, Chao Dong, Liang Lin, and Chen Change Loy. Crafting a toolchain for image restoration by deep reinforcement learning. In *Proceedings of the IEEE/CVF Conference on Computer Vision and Pattern Recognition (CVPR)*, 2018. 2
- [44] Ke Yu, Xintao Wang, Chao Dong, Xiaoou Tang, and Chen Change Loy. Path-restore: Learning network path selection for image restoration. *IEEE Transactions on Pattern Analysis and Machine Intelligence*, 44(10):7078–7092, 2022. 2
- [45] Roman Zeyde, Michael Elad, and Matan Protter. On single image scale-up using sparse-representations. In *Curves and Surfaces*, pages 711–730, Berlin, Heidelberg, 2012. Springer Berlin Heidelberg. 6, 7
- [46] Yulun Zhang, Kunpeng Li, Kai Li, Lichen Wang, Bineng Zhong, and Yun Fu. Image super-resolution using very deep residual channel attention networks. In *Proceedings of the European Conference on Computer Vision (ECCV)*, 2018. 1, 2
- [47] Yulun Zhang, Yapeng Tian, Yu Kong, Bineng Zhong, and Yun Fu. Residual dense network for image super-resolution. In *Proceedings of the IEEE/CVF Conference on Computer Vision and Pattern Recognition (CVPR)*, 2018. 1, 2, 3, 4, 6, 7
- [48] Shangchen Zhou, Jiawei Zhang, Jinshan Pan, Haozhe Xie, Wangmeng Zuo, and Jimmy Ren. Spatio-temporal filter adaptive network for video deblurring. In *Proceedings of the IEEE/CVF International Conference on Computer Vision (ICCV)*, 2019. 2